Author's personal copy

Chapter 37

Lahars and Their Deposits

James W. Vallance and Richard M. Iverson
US Geological Survey, Cascades Volcano Observatory, Vancouver, WA, USA

Chapter Outline

1. Introduction **650**
1.1. Historical and Prehistoric Examples of Lahars 650
1.2. Purpose 650
2. Genesis of Lahars **651**
2.1. Lahars Caused by Melting of Snow and Ice, Floods, or Heavy Rains 651
2.2. Lahars Caused by Collapse of Volcano Flanks 651
3. Lahar Behavior: A Mechanical Perspective **652**
3.1. Lahar Dynamics and Runout: Statistical Patterns 654
3.2. Lahar Dynamics and Runout: Physics-Based Models 654
4. Lahar Behavior: A Geological Perspective **656**
4.1. Erosion, Bulking, and Mass Growth 656
4.2. Grain-Size and Grain-Density Segregation 657
4.3. Downstream Dilution and Flow Transformation 658
5. Lahar Deposits **658**
5.1. Depositional Processes 658
5.2. Characteristics of Deposits 660
5.3. Distinguishing Lahar Deposits from Other Common Diamictons 664
Further Reading **664**

GLOSSARY

bulking The incorporation of solid debris, resulting in increased lahar mass and sediment concentration as the lahar moves downstream.

debris avalanche A flowing mixture of debris, rock, and moisture that moves downslope under the influence of gravity. Debris avalanches differ from debris flows in that they are not water-saturated and in that the load is mostly supported by particle-particle interactions.

debris flow A water-saturated mixture of debris that moves downslope under the influence of gravity, in which the solid and liquid fractions are approximately equal volumetrically and in which the two fractions move downstream approximately in unison.

debulking A process in which a lahar selectively deposits certain particles, owing to their size or density, as it moves downstream. Debulking differs from the general deposition of sediment because it preferentially removes particles, usually large or dense ones, from the flow. It results in decreased sediment concentration.

dilatancy A property of a granular material that enables it to change volume through expansion of pore space when subject to shear strain. Negative dilatancy implies pore space reduction.

hyperconcentrated flow A transitional flow type, between debris flow and streamflow. Unlike streamflow, a hyperconcentrated flow carries very high sediment loads, and unlike debris flow, coarse-grained solids tend to separate vertically from the liquid-and-fine-solids mixture.

granular temperature A scalar measure of random kinetic energy associated with grain agitation. Granular temperature may be interpreted as twice the fluctuation kinetic energy per unit mass of granular solids.

lahar An Indonesian term most commonly defined as a rapidly flowing, gravity-driven mixture of rock, debris, and water from a volcano. A lahar can vary in character with time and distance downstream. It may comprise one or more flow types, which include debris flow, transitional or hyperconcentrated flow, and muddy streamflow or flood flow. Flow-type transitions are commonly defined in terms of solids fraction; however, such transitions are gradational and dependent on other factors such as sediment-size distribution, clay mineralogy, particle agitation, and energy of the flow.

liquefaction A process that enables water-saturated sediment mixtures to flow almost as fluidly as liquids. Liquefaction results from excess pore-fluid pressure that reduces frictional energy dissipation at grain contacts. As pore-fluid pressure exceeds hydrostatic values such water-sediment mixtures become progressively more liquefied.

muddy streamflow or flood flow A type of flow in which fine-grained sediment moves in hydrodynamic suspension (suspended load) and coarse-grained sediment moves along the streambed (bed load). Some floods and muddy streamflows at volcanoes are genetically related to lahar events, but many are not.

stage (of flow) The surface height (above the channel bottom) of a flowing lahar or streamflow at a particular time. Examples

The Encyclopedia of Volcanoes. http://dx.doi.org/10.1016/B978-0-12-385938-9.00037-7
Published by Elsevier Inc. All rights reserved.

The Encyclopedia of Volcanoes, Second Edition, 2015, 649–664

Author's personal copy

of lahar stages include the initial rising or waxing stage, the peak-inundation stage, and the final long-duration falling or waning stage.

suspension (hydrodynamic) A state in which fine particles remain suspended in a liquid solely as a consequence of buoyancy, liquid viscosity, and Brownian forces. Fluid turbulence can assist hydrodynamic suspension, but it is not a requisite.

turbulence (hydrodynamic) Chaotic fluid movement or deviation of flow from laminar. Turbulent fluid flow characterizes streamflows but not debris flows or sediment-rich hyperconcentrated flows. Turbulence is generated by fluid momentum fluxes and differs from debris agitation that is measured by granular temperature.

1. INTRODUCTION

Lahars occur during volcanic eruptions—or, less predictably, through other processes on steep volcanic terrain—when large masses of water mixed with sediment sweep down and off volcano slopes and commonly incorporate additional sediment and water. Because lahars are water-saturated, both liquid and solid interactions influence their behavior and distinguish them from other related phenomena common to volcanoes, such as **debris avalanches** and floods. The rock fragments carried by lahars make them especially destructive; the abundant liquid contained in them allows them to flow over gentle gradients and inundate areas far away from their sources. People in such distal areas commonly neither expect the danger nor anticipate the destructive power of lahars.

1.1. Historical and Prehistoric Examples of Lahars

Lahars inundate areas surrounding volcanoes and can damage or destroy communities downstream. The 1985 pyroclastic eruption of Nevado del Ruiz in Columbia was a small event (0.01 km^3) but generated lahars 10 times larger ($\sim$0.1 km^3) that flowed as far as 100 km down four of five drainages that head at the volcano (Pierson et al., 1990). These, the deadliest historical lahars worldwide, destroyed more than 5000 homes and killed more than 23,000 people. In the town of Armero, 73 km downstream of the volcano, virtually all structures in the path of a lahar were obliterated and three-quarters of the inhabitants were killed. The interaction of hot pyroclastic flows or surges with glacial ice and snow at the summit of the volcano caused the Nevado del Ruiz lahars. By contrast, the 1980 eruption of Mount St Helens showed that large, destructive lahars form not only owing to the interaction of hot pyroclastic rock with snow and ice but also result from partial or wholesale **liquefaction** of water-laden debris-avalanche deposits (Scott, 1988).

Breakout of crater lakes and volcano-dammed lakes can cause large lahars during or after eruptions. Kelut volcano, on the island of Java in Indonesia, is notorious for producing lahars when explosive eruptions expel its crater lake, and its lahars are notorious for killing people who live on its fertile slopes and for destroying villages within a 40-km radius. Since 1848, the volcano has erupted 10 times. Of these eruptions, seven have expelled the crater lake, and five have produced devastating lahars. The most devastating of these lahars occurred when the largest volumes of water were expelled from the lake. In 1919, an eruption blew 4×10^7 m^3 of water out of Kelut's lake and generated lahars that swept almost 40 km downstream, covered more than 130 km^2, and killed more than 5000 people.

Torrential rains mobilized loose debris and generated hundreds of lahars for years after the 1991 Pinatubo eruption in the Philippines. Although most of the Pinatubo lahars were relatively small, within 6 years they cumulatively remobilized about 2.5 km^3 of the 5.5 km^3 of pyroclastic flows emplaced during the eruption. Filling of downstream channels as well as overbank flow onto surrounding fields and villages inundated more than 400 km^2 and displaced more than 50,000 persons.

In 1998, Hurricane Mitch unleashed torrential rain that caused a slope failure and released a flood of water that generated a lethal lahar at Casita volcano in Nicaragua (Scott et al., 2005). The flood of water and sediment eroded and incorporated three times its volume in sediment as it descended the steep volcano slopes. As it spread across the gentle slopes of the volcano's apron, the lahar destroyed two towns and killed more than 2000 inhabitants.

Studies of prehistoric lahar deposits reveal the potential for even greater disasters. About 5600 years ago, the 3.8-km^3 Osceola mudflow from Mount Rainier, USA began with an edifice collapse that transformed to a lahar. The lahar apparently mobilized because of the enormous volume of water contained in pore spaces and in the volcano's hydrothermal system (Vallance and Scott, 1997). It filled valleys to depths of 80–150 m, flowed more than 120 km down valleys, and continued as far as 20 km underwater in Puget Sound while retaining sufficient coherence to transport large gravel and wood fragments (Crandell, 1971). The 540 km^2 area it inundated is now populated by hundreds of thousands of people.

1.2. Purpose

The chief purpose of this chapter is to summarize what is known about the nature and behavior of lahars on the basis of observations, experiments, theory, and examination of deposits, and further to describe the nature of deposits derived from such events. Because the timing of lahar events is largely unpredictable and working with active flows can be hazardous, much of our present knowledge of flow behavior is inferred from the study of lahar deposits. Nonetheless, key observational, experimental, and theoretical studies have also improved understanding.

Author's personal copy

2. GENESIS OF LAHARS

Lahars may be primary (syneruptive) or secondary (posteruptive or unrelated to eruptions). Lahar genesis requires (1) an adequate water source; (2) abundant unconsolidated debris, which typically includes pyroclastic-flow and -fall deposits, glacial drift, colluvium, and soil; (3) steep slopes (commonly >25°) and substantial relief at the source; and (4) a triggering mechanism. Water sources include pore or hydrothermal water, rapidly melted snow and ice, subglacially trapped water, crater or other lake water, and rainfall runoff. Water encountered along a lahar's path, either in streams or lakes, or stored within floodplain sediments can also influence downstream dynamics.

2.1. Lahars Caused by Melting of Snow and Ice, Floods, or Heavy Rains

Floods of water moving across loose sediment common on the flanks and aprons of volcanoes readily incorporate that debris and may quickly form lahars (Figure 37.1(A) and (B)). This **bulking** process is critical to all lahars that begin with sudden water releases.

Lahars induced by sudden water release can occur by four principal means. (1) Hot rock avalanches, pyroclastic flows, and surges mix with and melt glacial ice and snow rapidly. Such hot flows may come entirely or nearly to rest, generating meltwater that then runs off, coalesces, and erodes the pyroclastic debris to form water-rich lahars. They may also continue moving across snow or ice, incorporating it continuously to form lahars that often include voluminous slurries of snow, ice, and slush. As they move downstream, the lahars may continue to bulk up with volcanic debris, glacial drift, alluvium, and colluvium so that within a few kilometers to several tens of kilometers they become solids-rich **debris flows**. Lahars of this type are considered primary. (2) Volcanic eruptions can displace large volumes of crater-lake water that form lahars downstream. Crater and caldera lakes and volcanic debris-dammed lakes can also break out months to years after eruptions. Such delayed breakouts occur when water levels gradually rise, then overtop or pipe through, and incise fragile debris dams rapidly. (3) Subglacial eruptions can form subglacial lakes that eventually break out when a section of the ice cap becomes buoyant or pervasively fractured and thereby releases the trapped water. Small-scale outburst floods also occur during periods of glacier ablation and commonly bulk up to form lahars. Huge eruption-driven outbursts cause sediment-rich water floods called jökulhlaups. (4) Lahars that result from intense rainfall often occur after eruptions deposit abundant loose debris from pyroclastic-flow or -fall deposits. Lahars of this type are commonly small but abundant during rainy periods. Size and frequency of rain-induced lahars may increase in the months or years following the primary pyroclastic eruption, then decrease exponentially as drainage networks and vegetation re-establish themselves (e.g., Mount Pinatubo after its 1991 pyroclastic eruption).

Because clay-rich sediment is both uncommon on the flanks or aprons of active volcanoes and resistant to erosion, lahars induced by sudden water release are generally clay-poor and contain less than about 5% clay/(sand + silt + clay) by dry weight.

2.2. Lahars Caused by Collapse of Volcano Flanks

Although most volcano flank collapses behave as debris avalanches, those with sufficient, widely dispersed pore water and hydrothermal water in the precollapse rock may liquefy as the material deforms during collapse. Flank-collapse-induced lahars may have various triggers, including magmatic or phreatic volcanism, volcanic or tectonic earthquakes, hydrothermal groundwater pressurization, and flank bulging caused by magma intrusion.

Hydrothermal alteration of rocks, especially at glaciated volcanoes, increases the probability of edifice-collapse lahars. Acid-sulfate leaching in hydrothermal systems removes mobile elements, adds sulfate, and decomposes framework silicates to form fine-grained silica phases, such as cristobalite and opal, and clay minerals, such as kaolinite and smectite. This process weakens the rock so that it more readily disintegrates during deformation after collapse. Thus, huge blocks of rock typical of debris avalanches are uncommon in lahars of this type. Abundant alteration minerals, especially clay minerals, increase porosity and decrease permeability of the rock and thus, in combination with the hydrothermal system, trap a widely dispersed reservoir of water within the precollapse rock mass. Because of its high water content and its tendency to disintegrate, hydrothermally altered rock, unlike fresh rock, easily liquefies as it deforms. Collapse-induced lahars are commonly clay-rich and most are observed to have greater than 5% clay/(sand + silt + clay) by dry weight (Vallance and Scott, 1997).

Clay-rich, collapse-induced lahars appear to be more common at ice-clad volcanoes than at volcanoes that are free of ice. Glacial erosion tends to expose deeper, potentially more-altered portions of volcanoes, while incised slopes in altered rock are susceptible to failure not only because the rock is weak but also because they are over-steepened. Lastly, melting glacial ice as well as seasonal snowpack provides a slow-release source of water that supplies the hydrothermal system and is important to the efficient operation of the acid-sulfate leaching process.

Author's personal copy

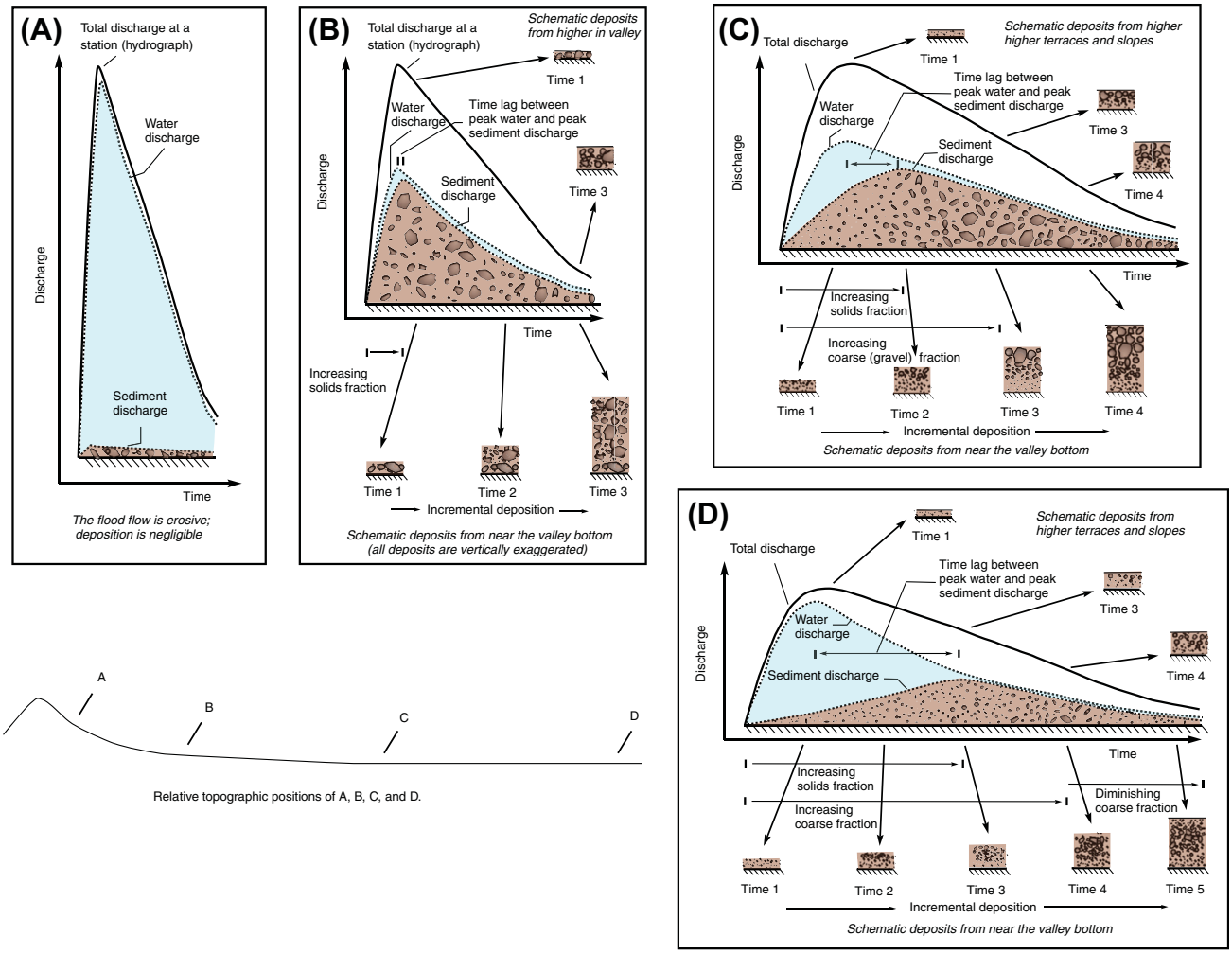

FIGURE 37.1 Schematic hydrographs showing how lahars beginning with water floods are initiated and behave as they undergo downstream dilution. (**A**) Flood flow; (**B**) Debris flow; (**C**) Transitional flow; (**D**) Hyperconcentrated flow. The diagram also illustrates the progressive-aggradation model of inverse grading in panels (**C**) and (**D**).

3. LAHAR BEHAVIOR: A MECHANICAL PERSPECTIVE

Lahars comprise roughly equal volumes of water and granulated rock, and their mechanical behavior can be understood by considering how this two-phase composition influences momentum transfer and energy dissipation (Iverson, 1997). When lahar mixtures flow, they can move almost like liquids—despite having grain concentrations and bulk densities comparable to that of solid ground. Lahar mobility can persist as long as water containing suspended mud-sized particles (silt + clay) reduces frictional energy dissipation by exerting local lubricating forces where large grains contact one another. On a continuum scale that encompasses many grains and adjacent fluid, effects of these local lubrication forces are manifested by pore-fluid pressures that may cause liquefaction. However, liquefaction diminishes as lahar motion slows and ceases, and lahar deposits ultimately dewater and consolidate until they reach a nearly rigid state (Major and Iverson, 1999). This conspicuous state transition provides clear evidence that lahar rheology is not a fixed property, but is instead dependent on solid-fluid interactions that evolve as a lahar's kinetic energy and composition evolve (Figure 37.2, Video 37.1).

Supplementary video related to this article can be found online at http://booksite.elsevier.com/9780123859389

In a continuum-mechanics context, the chief measure of lahar composition is the mixture bulk density ρ, defined as

$$\rho = \rho_s m + \rho_f (1 - m) \tag{37.1}$$

Author's personal copy

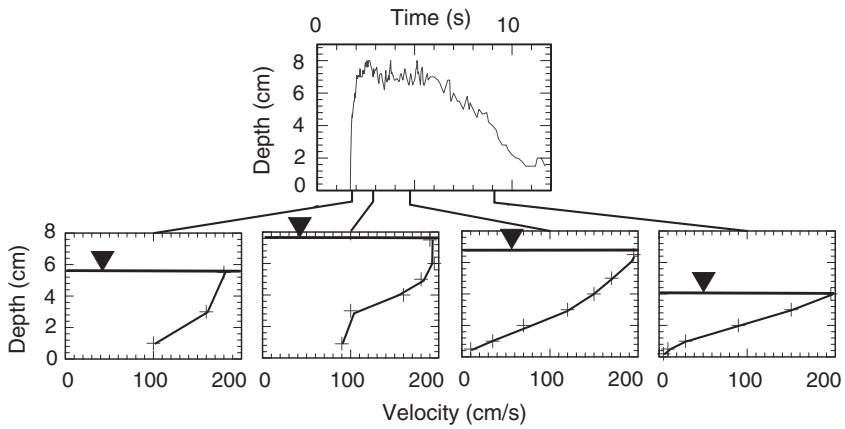

FIGURE 37.2 Variation of flow depths and vertical velocity profiles in experimental debris flow as it passed cross-section 3 m downslope from head of rectangular flume 0.3-m wide and sloped 18°. Variations in velocity profiles imply variation in apparent rheology. Flume bed roughened with grains like those used in flowing debris, 0.8–20 mm. Data extracted from analysis of video of flow past smooth glass walls. Volume fraction 0.5 at flow head, 0.45 flow tail. Black triangles indicate flow surface. *From Iverson and Vallance (2001). See Video 37.1 for an animated version of this figure.*

where ρ_s is the density of solid grains, ρ_f is the density of intergranular fluid (including clay and silt-sized particles held in **hydrodynamic suspension**), and m is the volume fraction occupied by all other solid grains. Typical values of these properties are $\rho_s \sim 2500$ kg/m^3, $\rho_f \sim 1100$ kg/m^3, $m \sim 0.6$, and $\rho \sim 2000$ kg/m^3, but some lahars can have values that differ greatly from these. For example, pumice-rich lahars can have $\rho_s \approx \rho_f$, implying that solid grains can float in the presence of hydrostatic fluid pressure. The values of m and ρ evolve by large amounts in many lahars as a consequence of bulking or **debulking**, while values of ρ_s and ρ_f may evolve in subtler fashion.

Like the bulk density ρ, the velocity $\vec{v}$ of lahar mixtures is defined by a weighted sum:

$$\vec{v} = [\vec{v}_s \rho_s m + \vec{v}_f \rho_f (1-m)]/\rho \qquad (37.2)$$

where $\vec{v}_s$ is the velocity of solid grains and $\vec{v}_f$ is the velocity of adjacent fluid. The weighted sum of the solid-phase momentum $\rho_s \vec{v}_s$ and the fluid-phase momentum $\rho_f \vec{v}_f$ per unit volume of mixture determines momentum per unit volume $\rho\vec{v}$ and dictates the form of (37.2) (Iverson, 1997). Equation (37.2) demonstrates that the mixture momentum $\rho\vec{v}$ can evolve as a result of evolution of m even if $\rho_s \vec{v}_s$ and $\rho_f \vec{v}_f$ remain constant.

Lahar materials generally remain well-mixed, implying that $\vec{v} \approx \vec{v}_s \approx \vec{v}_f$, but small differences between solid- and fluid-phase velocities can have large implications for momentum exchange and energy dissipation. These differences can be summarized by

$$\vec{q} = (\vec{v}_f - \vec{v}_s)(1-m) \qquad (37.3)$$

where $\vec{q}$ is the volumetric fluid flux per unit area in a frame of reference that moves with the adjacent solid grains. Nonzero values of $\vec{q}$ imply the existence of solid-fluid drag that may reduce grain-contact forces. For lahars that contain grains with a great variety of shapes and sizes, grain-scale drag forces cannot be determined precisely. However, on a bulk continuum scale drag forces can be estimated by using Darcy's law:

$$\vec{q} = -(k/\mu)\nabla p_e \qquad (37.4)$$

where k is the hydraulic permeability of the granular aggregate, μ is the viscosity of intergranular fluid, and p_e is the nonhydrostatic or "excess" fluid pressure. The pressure gradient ∇p_e generated by $\vec{q}$ arises from drag that is inversely proportional to k/μ. Values of k/μ for lahar materials range from about 10^{-4} m^{3}s/kg for dilute mixtures of water, sand, and gravel to 10^{-14} m^{3}s/kg for concentrated, mud-rich mixtures (Iverson, 1997). A mid-range value $k/\mu = 10^{-9}$ m^{3}s/kg in Equation (37.4) implies that a $\vec{q}$ value no larger than 10^{-5} m/s can produce a fluid pressure gradient ∇p_e in excess of a typical hydrostatic pressure gradient, $\rho_f\, g \approx 10^4$ kg/m^{2}s^2. Recognition that small $\vec{q}$ leads to excess fluid pressure gradients and that excess fluid pressure gradients govern liquefaction is crucial for understanding both the mechanics of lahars and the importance of changes in lahar composition that alter the value of k/μ. Increased proportions of silt and clay greatly diminish permeability, decrease k/μ, and thereby enhance lahar mobility (Video 37.2).

Supplementary video related to this article can be found online at http://booksite.elsevier.com/9780123859389

Excess fluid pressure gradients that counteract gravity-driven settling of grains cause at least partial liquefaction, thereby mimicking the effect of enhanced buoyancy and reducing intergranular friction. Such excess pressure gradients tend to dissipate with time if grain settling proceeds unperturbed, but any process that transiently dilates a lahar mixture can restart the settling process (Iverson and George, 2014). For example, as lahars descend steep channels or encounter obstacles, reduction of solids volume fraction m results from agitation of debris caused by conversion of large-scale translational kinetic energy to disorganized grain-scale kinetic energy (i.e., **granular**

Author's personal copy

temperature). Provided that sufficient fluid is available to fill intergranular voids that are enlarged by this agitation, the fluid can subsequently pressurize as ρ and m relax toward equilibrium values.

The mobility of lahar mixtures can thus be viewed as the product of an energy cascade that begins with the bulk gravitational potential energy of sediment and water poised at high elevations. The next step of the cascade entails transformation of potential energy into a combination of translational kinetic energy, granular temperature, and elevated fluid pressure. The cascade ends when friction has dissipated all of the original energy as heat and the lahar mixture comes to rest and consolidates (Iverson, 1997).

3.1. Lahar Dynamics and Runout: Statistical Patterns

Lahar mobility and dynamics on a large scale can be gauged from the extent of areas inundated downstream. In this context, the simplest measure of mobility is the ratio H/L, where H is the total vertical elevation lost and L is the total horizontal distance traversed during lahar motion. Although this measure is easy to understand and use, it disregards the important effects of lahar volume and three-dimensional path topography. Alternative measures of bulk mobility account for these effects by using scale-invariant power-law equations, $A = aV^{2/3}$ and $B = bV^{2/3}$, where A is the average vertical cross-sectional area inundated along a lahar path, B is the total planimetric area inundated, V is lahar volume, and a and b are statistically calibrated coefficients (Iverson et al., 1998). Values of a decrease while those of b increase as flows exhibit decreasing frictional resistance and increasing mobility. Indeed, values of a and b that are statistically calibrated using field data provide numerical indices that distinguish the mobility of lahars from less mobile debris avalanches (Figure 37.3). Calibrated values can vary for lahars with differing compositions and origins, but the values $a = 0.05$ and $b = 200$ apply to a broad spectrum of volcanic debris flows. As a result, the empirically calibrated inundation-area equations, $A = 0.05V^{2/3}$ and $B = 200\,V^{2/3}$, have proven useful for assessment of lahar hazards. The same empiricisms also provide a basis for testing some aspects of numerical models of lahar dynamics.

3.2. Lahar Dynamics and Runout: Physics-Based Models

The most powerful tools currently available for understanding lahar dynamics are depth-averaged numerical models. The equations used in these models are derived by applying the laws of mass and momentum conservation, but this application is simplified by assuming that momentum fluxes normal to the bed are negligible in comparison to downstream fluxes. Nevertheless, modern depth-averaged lahar models are sophisticated enough to simulate the primary features of lahar dynamics. For example, they can account for entrainment of bed or bank material that may change total lahar mass and solid volume fraction.

For downstream motion limited to one direction (here denoted by x), depth-averaged conservation of mass within a two-phase lahar that may erode its bed is described by Iverson (2013) as

$$\frac{\partial(\rho h)}{\partial t} + \frac{\partial(\rho h \bar{v})}{\partial x} = \rho_b \frac{\partial z_b}{\partial t} \tag{37.5}$$

where t is time, h is flow thickness, $\bar{v}$ is the depth-averaged value of the x-component of $\vec{v}$, $\partial z_b/\partial t$ is the local rate of bed lowering due to erosion in the direction normal to x, and ρ_b is the bulk density of bed material subject to erosion. The lahar bulk density ρ may evolve because of differences between ρ and ρ_b, and it may also evolve because of changes in mixture agitation that result in changes in the solid volume fraction m (Iverson and George, 2014).

Depth-averaged conservation of x-momentum in a lahar that obeys (37.5) is expressed by

$$\frac{\partial(\rho h \bar{v})}{\partial t} + \frac{\partial\left(\beta \rho h \bar{v}^2\right)}{\partial x} = \rho g_x h - L_x - \tau_b \tag{37.6}$$

where g_x is the x-component of the acceleration due to gravity, L_x is a resisting stress proportional to $g_z h[\partial(\rho h)/\partial x]$ that arises when gravity acts on a mass with an uneven weight distribution, τ_b is the resisting basal shear traction, and β is a momentum-distribution coefficient that accounts for deviations of v from $\bar{v}$ but is commonly assumed to equal 1. Importantly, (37.6) contains no term analogous to the bed-erosion term $\rho_b \partial z_b/\partial t$ in (37.5). Such a term is absent because static bed material lacks momentum to contribute to the lahar. However, a crucial and often overlooked implication of (37.6) is that, if $\rho\bar{v}$ is constant, then the value of τ_b in (37.6) must diminish as the rate of erosion increases, for otherwise momentum is not conserved in the two-body system comprising a lahar and its bed (Iverson, 2012). Indeed, relative to τ_b acting in the absence of erosion, τ_b must decrease by exactly the amount $\rho\bar{v}(\partial z_b/\partial t)$ to enable erosion at the rate $\partial z_b/\partial t$ to occur—provided that $\beta = 1$ applies and that the bed-normal momentum flux is zero. This inference helps explain why bed erosion and growth of lahar momentum commonly proceed hand-in-hand, but it does not explain the reasons for reduction of τ_b.

Phenomena that determine the evolving value of τ_b depend on the details of small-scale mixture dynamics and bed composition. Small-scale mixture dynamics generally involves some combination of energy-dissipating collisions and rubbing contacts of grains, as well as viscous fluid flow that simultaneously lubricates grain contacts and dissipates fluid kinetic energy. No complete model of these

Author's personal copy

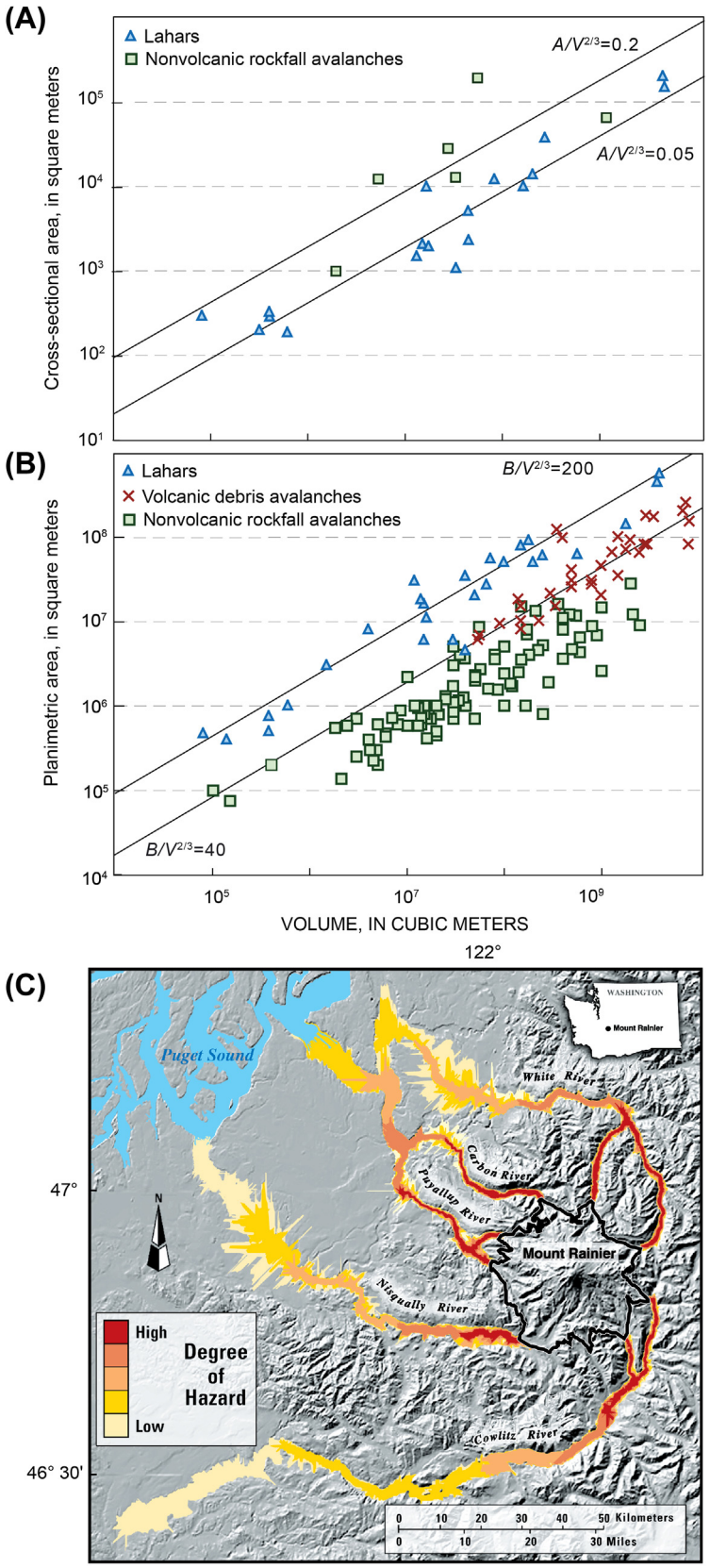

FIGURE 37.3 Plots of (**A**) inundated flow-path cross-sectional area *A* versus flow volume *V*, (**B**) area inundated *B* versus volume, and (**C**) inundation areas calculated for valleys draining Mount Rainier, Washington, USA. *(Details in Iverson et al. (1998).)*

Author's personal copy

interacting processes in complex lahar mixtures is available. However, where a lahar interacts with its bed, behavior can be approximated by using a modified Coulomb friction equation expressed as

$$\tau_b = \left[(\rho_s - \rho_f)g_z h - p_e\big|_{z_b}\right]\tan\phi(I_v) \qquad (37.7)$$

where g_z is the bed-normal component of gravitational acceleration, $(\rho_s - \rho_f)g_z h$ is the buoyant weight of granular debris acting on the bed, $p_e\big|_{z_b}$ is the excess pore pressure acting on the bed, and $\phi(I_v)$ is a Coulomb friction angle that increases gradually as a function of a dimensionless ratio I_v that compares the viscous resistance to volume change to total normal stress (Boyer et al., 2011). This parameter, defined here as

$$I_v = \frac{\mu(\bar{v}/h)}{(\rho_s - \rho_f)g_z h - p_e\big|_{z_b}}, \qquad (37.8)$$

accounts implicitly for the influences of collisional and viscous energy dissipation on Coulomb friction. These influences grow as the shear rate increases and as the effect of gravity-induced stresses decreases. If $I_v = 0$, then $\phi(I_v)$ equals the static friction angle, which for most sediment ranges from 30 to 40°. As $I_v \to \infty$, values of $\phi(I_v)$ increase but are unlikely to exceed about 60°.

Equations (37.7) and (37.8) imply that a reduction in τ_b accompanying bed erosion might occur for several reasons. For example, undrained loading of wet bed sediment overridden by a lahar might increase $p_e\big|_{z_b}$. In extreme cases such an increase can lead to wholesale bed liquefaction and a drastic reduction in τ_b (Iverson et al., 2011). A subtler but nevertheless important effect can arise when fast-moving, overriding lahar material with a relatively large value of $\phi(I_v)$ interacts with static or slightly moving bed material with a smaller value of $\phi(I_v)$. In this case, τ_b acts on a surface that migrates downward into effectively weaker material as erosion proceeds, thereby diminishing the basal shear resistance.

The mathematical description of lahar motion given by (37.5), (37.6), and (37.7) is incomplete without equations that describe evolution of $z_b(x,t)$, $p_e\big|_{z_b}(x,t)$, and $\rho(x, t)$ (or, alternatively, $m(x, t)$). Various rationales have been offered for formulating such equations, but research has not yet identified the best option. Thus, for the present, all mathematical models of lahar dynamics remain unfinished or, at least, unproven. Many models simply assume that $\rho(x,t)$ is constant and that $z_b(x,t)$ and $p_e\big|_{z_b}(x,t)$ are known independently.

4. LAHAR BEHAVIOR: A GEOLOGICAL PERSPECTIVE

Lahars commonly change character as they travel downstream (Figure 37.1). Floods generated on or near volcanoes can incorporate enough sediment proximally to become **hyperconcentrated flows** or debris flows. In medial or distal reaches, lahars that move down river channels push water ahead of them such that sediment-rich debris flows lag behind water-rich hyperconcentrated flows and flood flows (Figure 37.4). Furthermore, debris avalanches descending the flanks of volcanoes can partly or entirely evolve to debris flows as they move downstream (Scott, 1988; Vallance and Scott, 1997).

4.1. Erosion, Bulking, and Mass Growth

Lahars cause erosion by undercutting steep slopes and terrace scarps and by scouring their beds. Erosion is strongest along steep channel reaches underlain by loose clastic sediment and weakest either along reaches underlain by highly resistant bedrock or reaches with gentle gradients. Along any particular reach, watery sediment floods and water-rich, hyperconcentrated flows are typically more erosive than sediment-rich flows (Video 37.3, Figure 37.4), but local erosion can occur regardless of flow type. The waxing stage of a lahar is likely to coincide with the most widespread and voluminous erosion and bulking. The final, waning stages of a lahar can also be erosive, and commonly result in channel incision of fresh lahar deposits as the flow becomes more watery.

Supplementary video related to this article can be found online at http://booksite.elsevier.com/9780123859389

Erosion at the base of a lahar occurs by piecemeal dislodgment of particles, by liquefaction of loose wet substrate and wholesale incorporation of that sediment, and by rip up of sediment owing to root throw of falling trees. The presence of undisturbed, delicate deposits such as tephra layers at the base of debris-flow deposits suggests that bed erosion is minimal in some topographic settings, especially when the flow type is a sediment-rich debris flow.

An important means by which lahars may incorporate sediment is by compression of loose wet substrate material and subsequent liquefaction of that material. As a lahar overruns wet or water-saturated sediment, it loads, compresses, and shears it slightly, and thereby drives up pore-fluid pressure, causing runaway liquefaction (Video 37.4) (Iverson et al., 2011). Pervasive liquefaction of substrate not only makes that sediment easily eroded and entrained, but also lubricates the base of the flow and allows it to accelerate downstream. Given more than a meter of precipitation during Hurricane Mitch at the end of the 1998 rainy season, the landslide-induced Casita lahar probably owed its downstream growth in volume (times 2–3) and its enhanced mobility to loading and liquefaction of water-saturated sediment in its path.

Author's personal copy

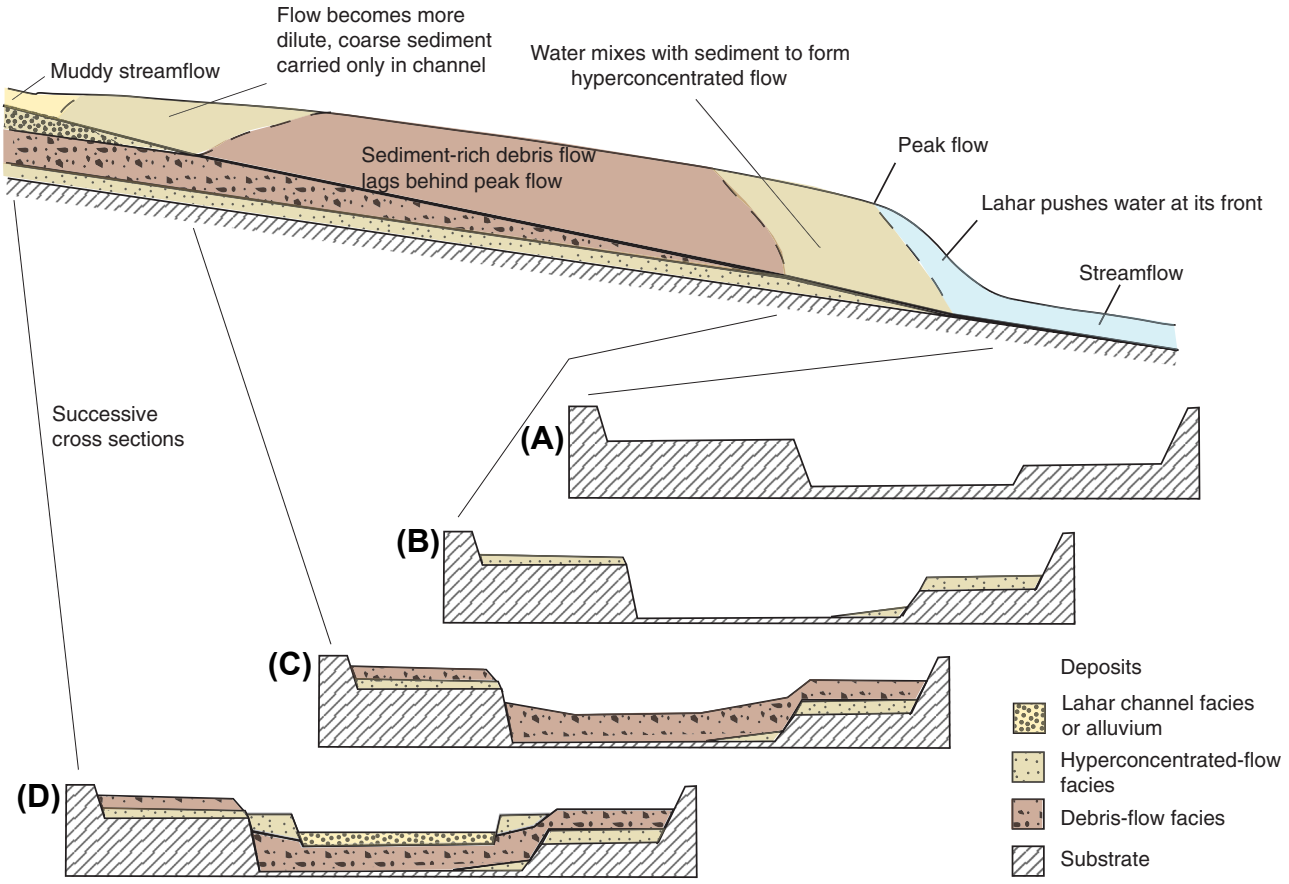

FIGURE 37.4 Schematic illustration of a lahar undergoing downstream dilution from debris-flow phase to hyperconcentrated-flow phase and deposit facies. The model shows the expected sequences of hyperconcentrated- and debris-flow deposits in cross-section ((**A**) through (**D**)).

Supplementary video related to this article can be found online at http://booksite.elsevier.com/9780123859389

Lahars voluminous enough to escape channels knock trees down and incorporate them. Root balls of falling trees drag considerable sediment into the active flow and loosen even more sediment that is then available for erosion. Voluminous lahars that inundate large areas of forested terrain can incorporate considerable quantities of sediment and huge amounts of wood in this way.

Undercutting of steep slopes, fluvial terrace scarps, and active stream banks is one of the most important ways in which lahars erode and incorporate sediment. Undercutting is active during flood flow, hyperconcentrated flow, and debris flow. Large lahars are capable of incorporating megablocks (>10 m across) of unconsolidated sediment, and sometimes even of bedrock, in this way (Figure 37.5). Megablocks may move tens of kilometers downstream before they ultimately fragment into smaller pieces.

Progressive downstream bulking causes downstream changes in lahars. Bulking adds sediment and thereby transforms flood flows and hyperconcentrated flows to more sediment-rich debris flows (Figure 37.1(A) to (B)). If the process continues, both waxing and waning **stages of flow** ultimately become debris flows. With continued downstream motion, debris flows become richer in exotic sediment such as alluvium, colluvium, and glacial drift. Study of deposits indicates that the waxing flow-front and following peak stages of the flow are the most erosive and thus most readily incorporate exotic sediment (e.g., Vallance and Scott, 1997). The sediment-rich falling flow that follows peak flow is less erosive and commonly deposits sediment rather than erodes it (Figure 37.1). The final waning-stage flow is typically more watery, and more erosive, but less voluminous in discharge than the preceding stage. Final waning stages of lahars commonly incise previously emplaced lahar deposits (Figure 37.4).

4.2. Grain-Size and Grain-Density Segregation

Grains in lahars can effectively segregate by density or size, but the most important segregation processes are mediated

Author's personal copy

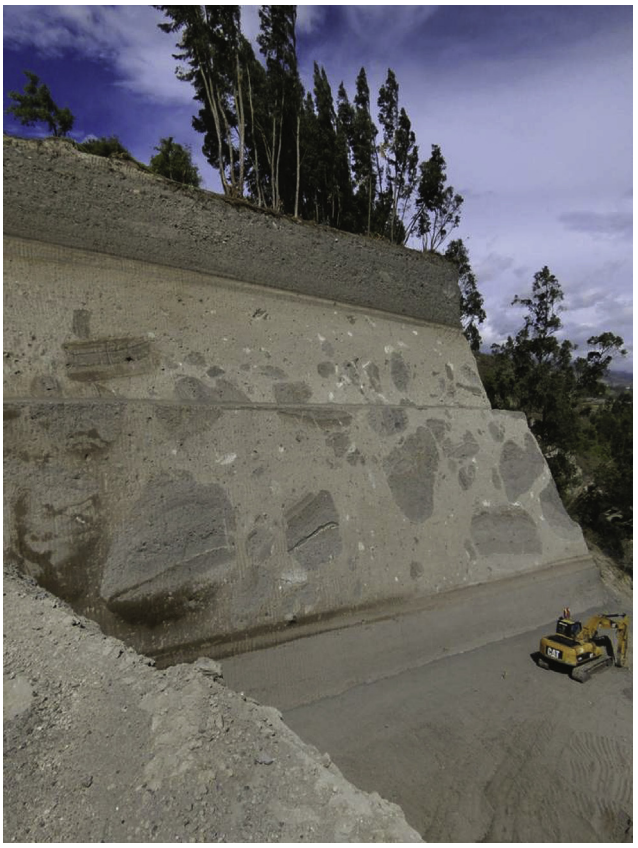

FIGURE 37.5 Photograph of cross-sectional view of 20-m thick lahar deposit about 40 km downstream from Cotopaxi, Ecuador, illustrating megaclasts incorporated into lahar by undercutting of channels. Megaclasts are mostly derived from earlier lahar deposits and are rounded from abrasion and rolling during flow. *Photograph by Patty Mothes.*

by the solids fraction m, proportion of coarse grains, and the fluid density ρ_f, the latter being determined by the proportion of mud-sized grains held in hydrodynamic suspension. In dilute lahars, large dense grains may readily settle gravitationally. Through this process, the largest grains collect in the lowest layer of a moving flow and progressively smaller ones collect above that; thus a normally graded flow develops. As larger grains collect toward the base of the flow where velocity is less than average, they progressively lag farther behind the flow front (Figure 37.1(C) to (D)).

In flows with greater solids fraction, grain-to-grain contacts inhibit gravitational settling and may favor preferential rise of large grains, even dense ones. In shearing flows with grains denser than the fluid and with solids fraction $> \sim 0.4$, large particles rise rather than settle. Force imbalances or grain rotations can push the large grains from one layer into another, and smaller grains are likely to fill in beneath larger ones and thus not rise. Once near the flow surface where velocity is greater than at the flow front, large grains migrate forward. Accretion of large grains at flow perimeters generates bouldery flow fronts (Figure 37.6). The mixture that follows the bouldery front remains fluid so that debris flows moving across fans and channels commonly develop resistant bouldery levee margins and liquefied interiors that govern their behavior (Iverson, 1997) (Videos 37.1 and 37.2, Figure 37.6).

4.3. Downstream Dilution and Flow Transformation

Once off the volcano's slopes, lahars commonly descend river channels that contain significant volumes of water. Lahars, which typically move faster than normal streamflow, push river water ahead of them and gradually, with distance downstream, begin to mix with that water (Pierson and Scott, 1985; Cronin et al., 1997). As the flow front becomes progressively more watery, it loses its capacity to carry larger gravel particles, and these progressively lag behind the flow front (Figures 37.1 and 37.4). With time and distance downstream, a dilution front progresses from the front of the lahar to its middle and eventually the entire lahar becomes more dilute. In lahars that occurred at Mount St Helens in 1980 and 1982, downstream dilution occurred over the course of tens of kilometers and caused a complete transformation from debris flow to hyperconcentrated flow (Figure 37.1(D)). In medial reaches, the hyperconcentrated flow preceded the debris-flow portion of the lahar because the dilution process began at the flow front, then gradually worked backward toward the tail as the flow traveled downstream (Figure 37.1(C)). Although downstream dilution can affect large lahars, the process has little effect on the behavior of lahars so large that their volumes are significantly greater than that of the water in the river being overrun.

5. LAHAR DEPOSITS

5.1. Depositional Processes

An increasing body of evidence indicates that deposits of both hyperconcentrated flows and debris flows aggrade progressively. Stratification in deposits of transitional or hyperconcentrated flows is clear evidence of progressive aggradation. Experimental observation of levees forming during debris flow emplacement shows that levees accrete from bottom to top (Major, 1997). Even in massive lahar deposits, field evidence of progressive aggradation is strong, including (1) strong alignment of elongate clasts parallel to flow directions, (2) imbrication of elongate clasts dipping upstream, (3) strong changes in composition of particles with vertical position in outcrops, especially those that are graded, and (4) marginal deposits with grain compositions similar to those at the base of thick valley-bottom deposits (Vallance and Scott, 1997). Lahars with

Author's personal copy

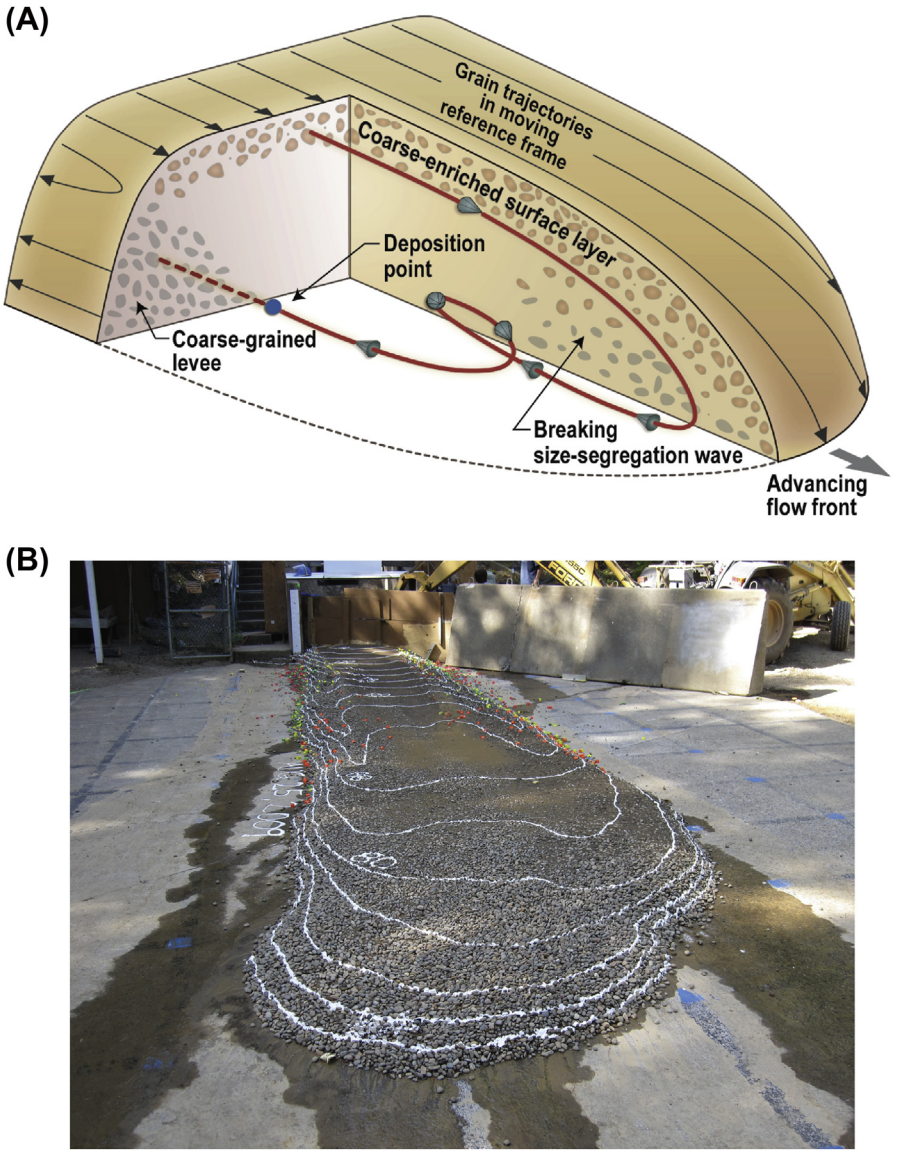

FIGURE 37.6 (**A**) Schematic cutaway illustration of the process leading to formation of lateral levees behind a debris flow front. Red path shows how coarse grain near surface migrates toward a levee. Reference frame moves at speed of advancing flow so that grain advancing less rapidly than flow front appears to move backwards (Johnson et al., 2012, gives details). (**B**) Deposit of experimental debris flow illustrating coarse-grained margins and levees. Width of distal end of deposit is about 2.5 m. White lines are topographic contours.

massive valley-bottom deposits sometimes show bottom-to-top compositional trends that mirror trends in deposits from successively higher to lower positions along valley margins. Such compositional trends imply progressive aggradation of a flow that evolves compositionally with time as it passes. In such cases, marks of peak-flow levels high on valley sides commonly indicate flow depths 5–10 times greater than typical valley-bottom deposit thicknesses.

In lahars, normally and inversely graded deposits generally originate from progressive aggradation of a flow that is compositionally zoned in terms of its grain-size distribution from front to tail of its hydrograph (Figures 37.1 and 37.7) rather than from a vertically graded flow that freezes in place. Figure 37.7(A) and (B) **(Times 1–4)** illustrates schematically how progressive aggradation from a debris-flow wave with a concentration of large particles at its front can generate a normally graded deposit (c.f., Vallance and Scott, 1997). Accretion occurs for a short time only near inundation limits where grading does not occur (Figure 37.7(B)**, Times 1–2**).

Progressive aggradation from a lahar wave that has become more dilute and less capable of carrying larger particles, which lag behind, emplaces inversely graded deposits (Figure 37.1(C) and (D)). Aggradation from a dilute debris flow whose grain-size distribution coarsens from its head toward its tail produces inversely graded deposits, which may be faintly stratified to massive (Figure 37.1(C)). Farther downstream, where the entire lahar has become hyperconcentrated, progressive aggradation produces finer grained beds that may be inversely graded or both inversely graded and normally graded (Scott,

Author's personal copy

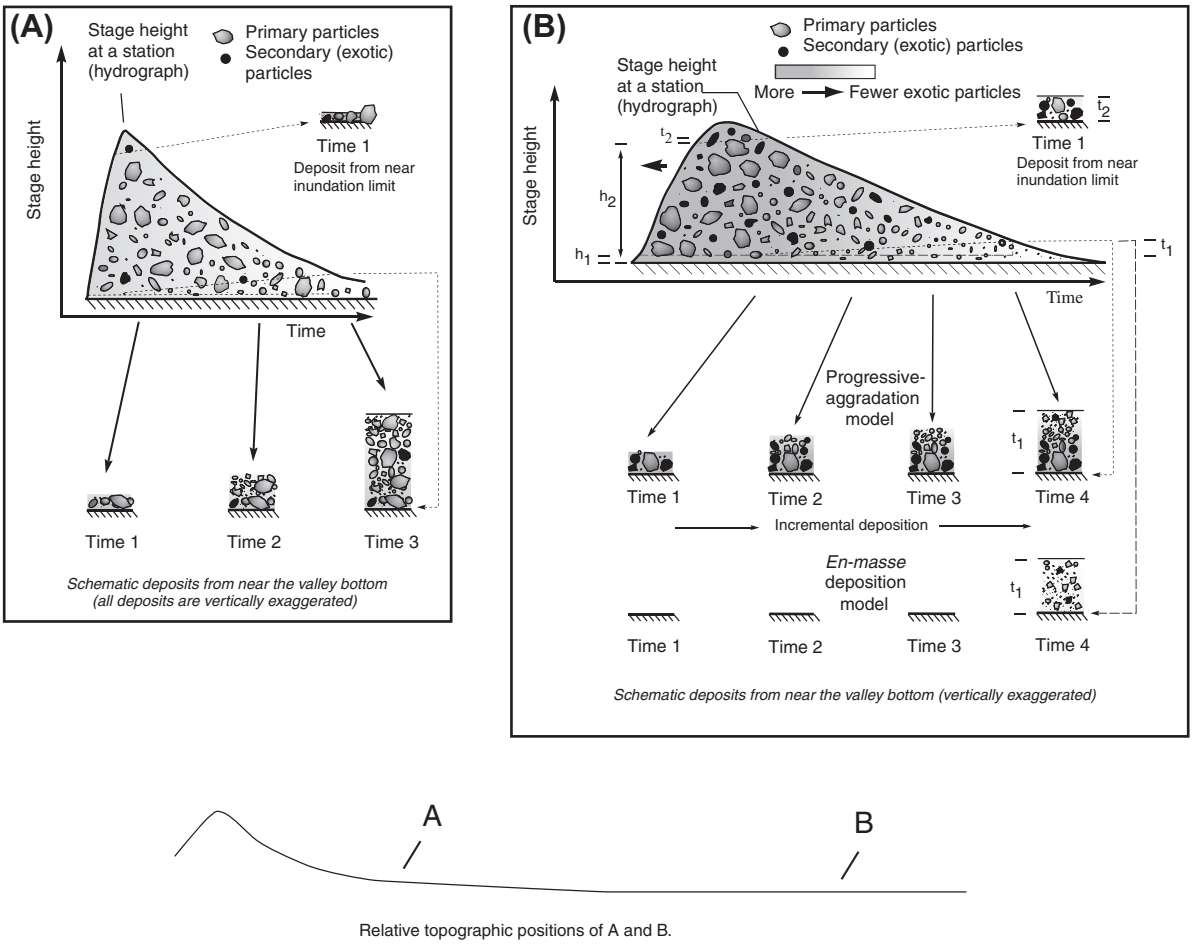

FIGURE 37.7 Schematic hydrographs showing the behavior and downstream changes of lahars that begin as avalanches of water-saturated debris. With increasing distance downstream ((**A**) to (**B**)) the lahar incorporates secondary exotic particles, especially near its flow front. Panel (**B**) also illustrates how a flow, coarser grained at its head than at its tail, can accrete incrementally to form a normally graded deposit. *(Adapted from Vallance and Scott, 1997.)* In (**B**), exotic particles are most common at the base of the normally graded deposits and at inundation limits.

1988) (Figure 37.1(D)). Deposits in positions higher on valley walls can also be graded, but often less obviously so.

Small bouldery debris flows that do not undergo downstream dilution commonly form cobble- and boulder-rich margins owing to the size segregation process described above (Figure 37.6). When a debris flow of this type reaches sufficiently gentle slopes, the frictional perimeter slows to a stop and leaves behind a steep-fronted fines-poor margin and a partly liquefied fines-rich interior. Upstream, the fluid interior drains downslope, leaves behind coarse margins, and forms levees (Johnson et al., 2012) (Figure 37.6(A)).

5.2. Characteristics of Deposits

Lahar deposits formed by debris flows, and hyperconcentrated flows that commonly evolve from them, have some similarities, but they have many differences too, and it is useful to characterize each type of deposit separately.

Debris-flow deposits are massive and very poorly sorted to extremely poorly sorted (greater than 2 phi units and typically greater than 4 phi units on the Wentworth scale). Grain-size distributions are commonly bimodal (Figure 37.8). The deposits may be normally (Figure 37.9) or inversely (Figure 37.10(A)) graded throughout or, in some cases, can be inversely graded near their bases and normally graded near their tops (Figure 37.10(B)). Sedimentary fabrics, such as imbrication, are weakly developed. Deposits are extremely compact. Particles found within debris-flow deposits can be monolithologic but are more commonly heterolithologic; they can be rounded to angular, but primary particles are usually subangular to angular. Deposits commonly exhibit vesicles in the matrix, which result from entrapment of air bubbles. Other common constituents include wood fragments, casts of wood fragments, and charcoal. Concentrations of coarse particles, especially low-density particles like pumice, are common at deposit tops.

Author's personal copy

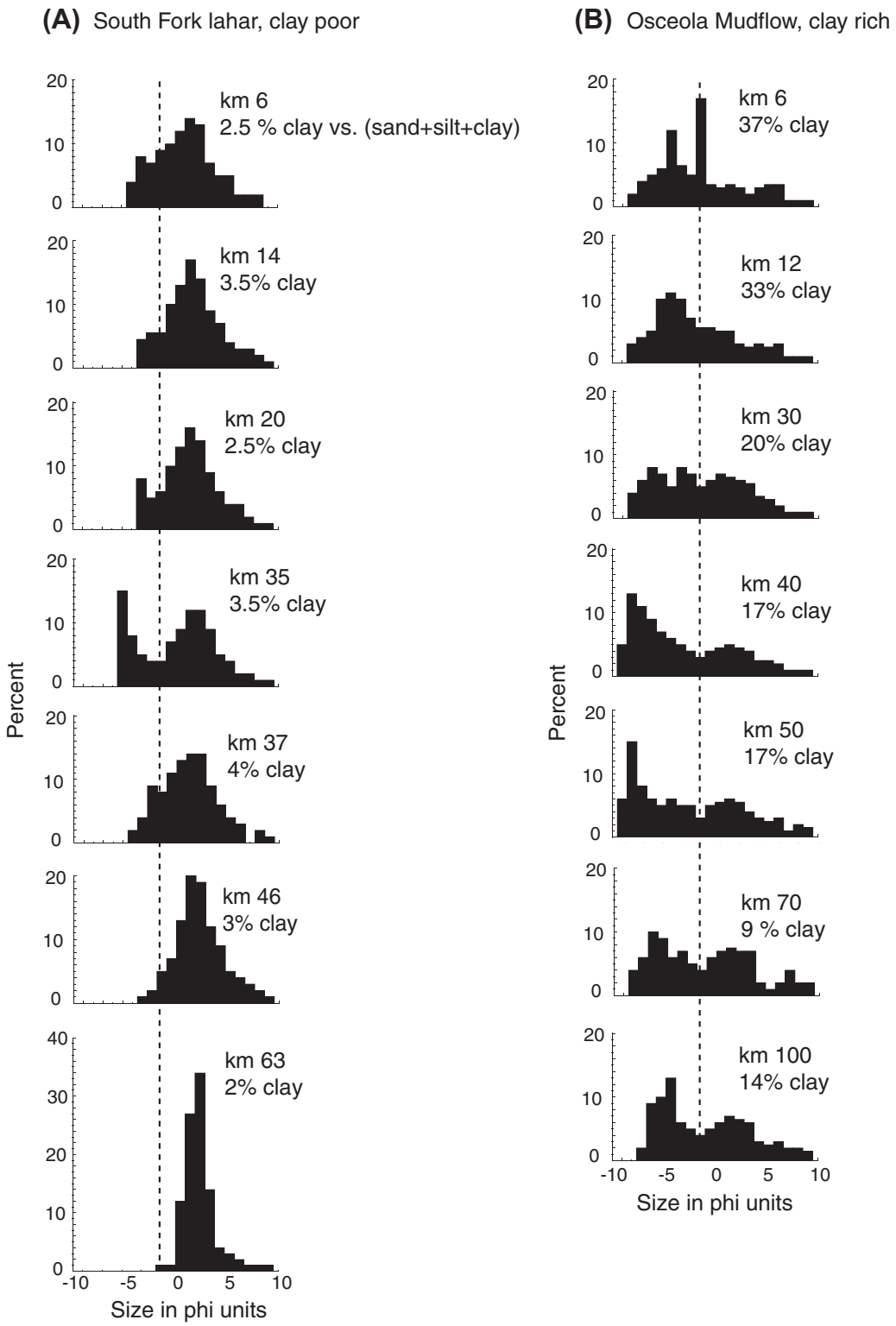

FIGURE 37.8 Grain-size histograms of (**A**) clay-poor South Fork Toutle River lahar. *From Scott (1988)* and (**B**) clay-rich Osceola lahar *From Vallance and Scott, 1997* sediment showing downstream trends. Also shown are proportions of clay in the deposit matrix (sand + silt + clay). In these examples, matrix clay percentage changes little downstream for clay-poor lahar deposit but falls nearly three-fold in clay-rich deposit. Vertical dotted line is at −2 phi units, or 4 mm size, and serves to highlight coarser and finer grained components.

Author's personal copy

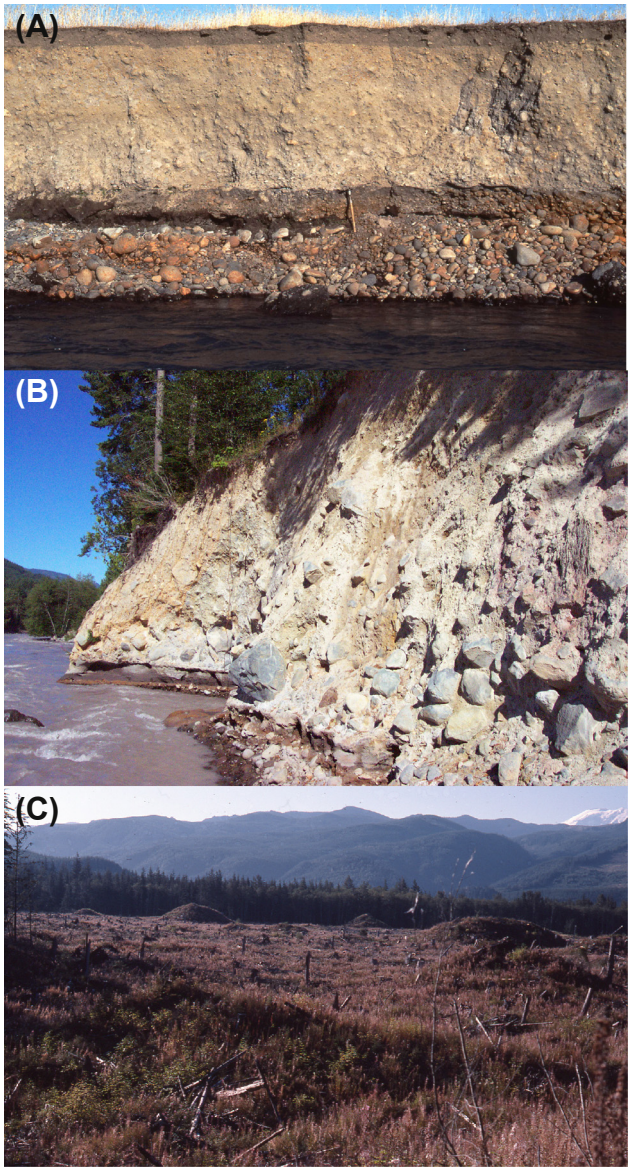

FIGURE 37.9 Photographs of clay-rich lahar deposits caused by volcano flank collapses. (**A**) Trout Lake lahar, Mount Adams, USA and (**B**) Osceola mudflow, Mount Rainier, USA illustrate normally graded debris-flow deposits. (**C**) Hummocks 20–40 m across and 10–15 m high characterize the surface of the Osceola mudflow, derived from Mount Rainier, USA, in the background 70 km upstream. Clay-rich normally graded deposits, locally with hummocks scattered across their surfaces, are common in collapse-induced lahars.

Thicknesses of debris-flow deposits vary from tens of centimeters to tens of meters. Thick fill deposits occur in valley bottoms and lowlands (Figures 37.5 and 37.9(B)). Deposits on higher terraces and slopes within valleys are thinner than those in valley bottoms, and those on steep slopes will drape underlying topography as thin veneers. Both levees and steep terminal flow fronts are common in the deposits of debris flows relatively unaffected by downstream dilution.

Hyperconcentrated-flow deposits have characteristics intermediate between debris-flow and alluvial deposits. They thus have intermediate sorting coefficients (1–2 phi units) and grain sizes. They can be massive (Figure 37.10(C)), but commonly they have weak stratification defined by thin horizontal beds and very low-angle cross bed-sets composed of fine-grained laminae and thicker coarser-grained beds (Figure 37.10(D)). Overbank deposits have grain sizes in the granule, sand, and silt range with the occasional isolated pebble, cobble, or boulder (Figure 37.10(E)). If pumice was an important constituent of the flows, zones of nearly 100% pumice are commonly present at the tops of overbank deposits. These pumice concentrations result from pumice rafts stranded during falling-stage hyperconcentrated flow. Channel-facies deposits commonly exhibit strong bimodality and clast support, with concentrations of cobbles and boulders surrounding granule-sand-silt matrix (Figure 37.10(E)). Vesicles are sometimes present but less obvious than in debris-flow deposits. Deposits are compact except for bouldery channel examples (Figure 37.10(E)). Though rare, dewatering features such as dish structures (Figure 37.10(G)) and pillar structures may be present.

Hyperconcentrated-flow deposits have flat tops and may vary in thickness from a few centimeters to several meters. Flow tops have scattered pebbles and large grains, especially pumice if present; they also commonly have thin layers of fine sand and silt that form during compaction and dewatering.

Lahar deposits fall into clay-rich and clay-poor groups (Figure 37.8), which empirically correspond to origins as avalanches of water-saturated hydrothermally altered rock and origins as flood of water incorporating loose sediment on the volcano. Lahar size, origin, and depositional environment determine the facies that form. Clay-rich lahar deposits at Mount Rainier are solely from avalanches. Such deposits are massive, extremely poorly sorted, and commonly normally graded (Figure 37.9(A) and (B)). The Osceola mudflow for example, has proximal and medial hummocky facies that contain many megaclasts (Figure 37.9(C)). Proximal and medial valley-side facies form thin (0.1–1 m) veneers on steep slopes; and proximal, medial, and distal axial facies form thick (2–20 m) fills with common normal grading in valley bottoms and lowlands. Clay-poor lahar deposits, such as those at Mount St Helens, may have the following facies (Figure 37.10): debris-flow (**A**), flood-plain (**E**), channel (**E**) transition (**B**), hyperconcentrated-flow (**C, D, G**), and stream-flow (**F, H**). The last three of these facies characterize downstream dilution of the lahar. Deposit interiors are more uniform, massive, poorly sorted, and matrix-rich than levees and snouts. Deposits left on steep upland slopes typically form thin lags with concentrations of the coarsest, densest particles, and a deficiency of matrix.

Author's personal copy

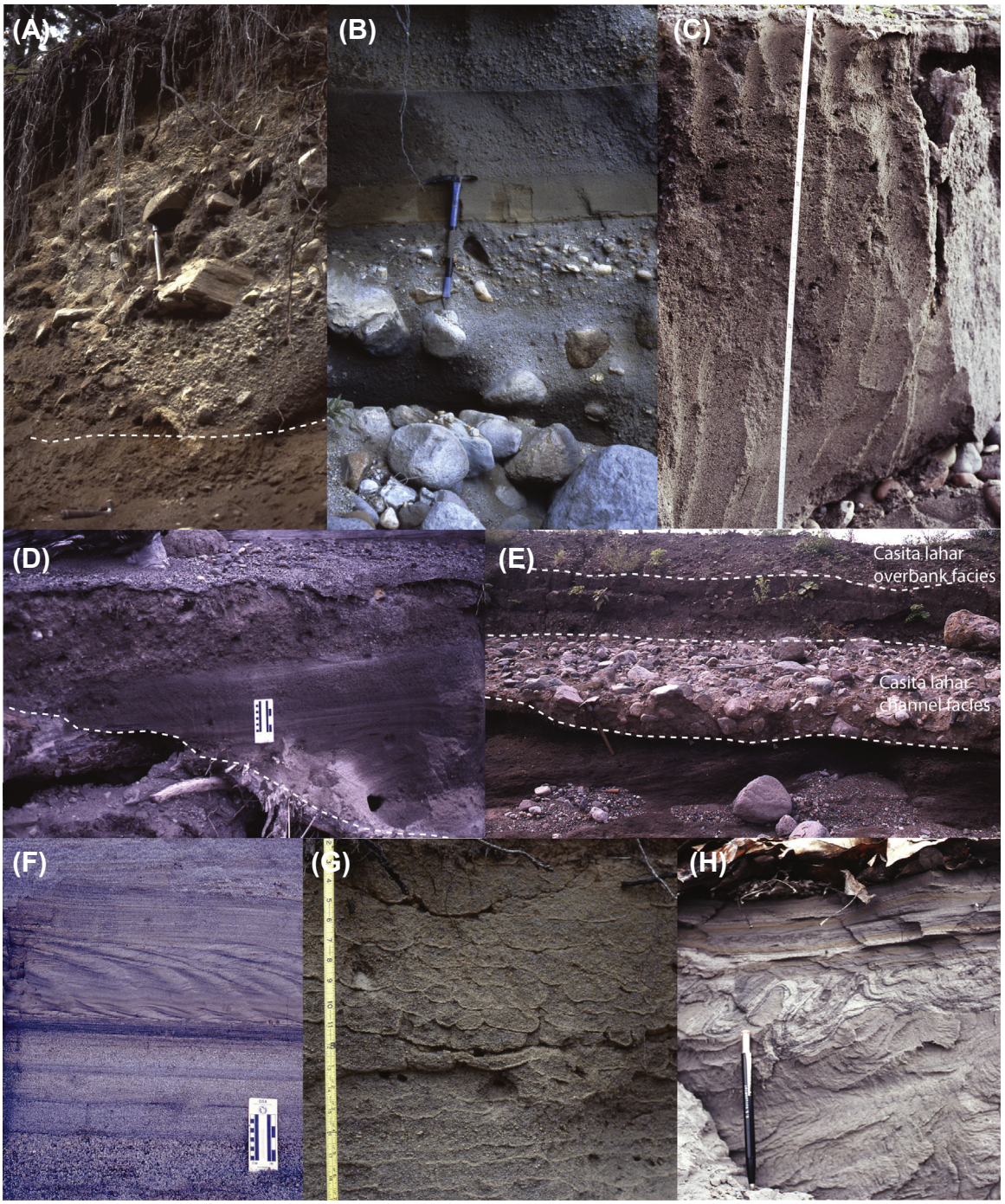

FIGURE 37.10 Photographs showing depositional facies of clay-poor lahars. (**A**) Clay-poor debris-flow deposit at Mount Adams, USA that is inversely graded at its base and both massive and ungraded at its top (dashed line indicates base of deposit; shovel is 50 cm long). (**B**) Transitional debris-flow to hyperconcentrated-flow deposits at Mount Rainier, USA. The basal unit (at the point of the ice axe) contains floating, rounded cobbles and boulders and probably reflects deposition from hyperconcentrated flow in a channel. (**C**) Hyperconcentrated-flow deposit that is inversely graded in the lowest two-thirds of the outcrop and normally graded in the upper third of the outcrop at Mount St Helens in 1982. The deposit comprises silt, sand, granules, and small pebbles with a single mode of coarse sand and granules. Deposit is about 1 m thick. (**D**) Faintly stratified hyperconcentrated-flow deposit and overlying transitional debris-flow deposit at Mount St Helens in 1982. (**E**) 1998 Casita lahar deposit, Nicaragua, illustrating lahar overbank and channel facies. (**F**) Climbing ripple structure transitioning upward to faintly stratified hyperconcentrated-flow facies at Pinatubo, Philippines. (**G**) Dish structure in a hyperconcentrated-flow deposit at Mount Rainier, USA. The structure evolves during or after deposition owing to dewatering during compaction. Structures are more strongly inflected toward the top of the unit. Tape measure for scale. (**H**) Wet-sediment deformation features in stream-flow facies of South Fork Toutle River lahar, 1980, Mount St Helens, USA. *((C), (G), and (H), photographs by Kevin Scott.)*

Author's personal copy

5.3. Distinguishing Lahar Deposits from Other Common Diamictons

No single characteristic serves to distinguish lahar deposits from those of nonwelded pyroclastic flows, glaciers, debris avalanches, and landslides. Unlike lahar deposits, nonwelded pyroclastic-flow deposits do not have matrix vesicles, are not as well cemented, and contain mainly juvenile particles. Carbonized wood and magnetically oriented clasts help to distinguish them from deposits of cold lahars (the vast majority) but not necessarily from those of hot lahars. Nonwelded pyroclastic-flow deposits are usually more friable than lahar deposits. Debris-avalanche deposits generally have surfaces that are more irregular than those of lahar deposits. Although lahar deposits, especially clay-rich ones, can have hummocks and lateral levees, these features are more prominent in debris-avalanche deposits. Distal and marginal parts of debris-avalanche deposits can be flat-topped and can contain matrix vesicles, but these features are more typical of lahar deposits. Lateral and terminal moraine landforms or striated boulders and cobbles within deposits distinguish till from lahars. Unlike lahar deposits, till does not contain matrix vesicles, casts of wood fragments, or the wood fragments themselves. Till is also more heterolithologic than most lahar deposits. Landslide deposits generally have more local distribution, and more uniform lithology than lahar deposits do. Mapping distribution and inferring context is perhaps the best way to distinguish among poorly sorted deposits common at volcanoes.

FURTHER READING

Boyer, F., Guazzelli, E., Pouliquen, O., 2011. Unifying suspension and granular rheology. Phys. Rev. Lett. 107, 188301. http://dx.doi.org/10.1103/PhysRevLett.107.188301.

Crandell, D.R., 1971. Postglacial Lahars from Mount Rainier Volcano, Washington. U.S. Geological Survey Professional Paper 677, 75 p.

Cronin, S.J., Neall, V.E., Palmer, A.S., Lecointre, J.A., 1997. Changes in Whangaehu river lahar characteristics during the 1995 eruption sequence, Ruapehu volcano, New Zealand. J. Volcanol. Geoth. Res. 76, 47–61.

Iverson, R.M., 1997. The physics of debris flows. Rev. Geophys. 35 (3), 245–296.

Iverson, R.M., 2012. Elementary theory of bed-sediment entrainment by debris flows and avalanches. J. Geophys. Res. 117, F03006. http://dx.doi.org/10.1029/2011JF002189, 17 p.

Iverson, R.M., 2013. Mechanics of debris flows and rock avalanches. In: Fernando, H.J.S. (Ed.), Handbook of Environmental Fluid Dynamics. CRC Press, Taylor and Francis, pp. 573–587.

Iverson, R.M., George, D.L., 2014. A depth-averaged debris-flow model that includes the effects of evolving dilatency: 1. Physical basis. Proceedings of the Royal Society, London, Series A, 470, 20130819. http://dx.doi.org/10.1098/RSPA20130819.

Iverson, R.M., Reid, M.E., Logan, M., LaHusen, R.G., Godt, J.W., Griswold, J.G., 2011. Positive feedback and momentum growth during debris-flow entrainment of wet bed sediment. Nat. Geosci. 4 (2), 116–121. http://dx.doi.org/10.1038/NGEO1040.

Iverson, R.M., Schilling, S.P., Vallance, J.W., 1998. Objective delineation of lahar-inundation hazard zones. Geol. Soc. Am. Bull. 110, 972–984.

Iverson, R.M., Vallance, J.W., 2001. New views of granular mass flows. Geology 29, 115–118.

Johnson, C.G., Kokelaar, B.P., Iverson, R.M., Logan, M., LaHusen, R.G., Gray, J.M.N.T., 2012. Grain-size segregation and levee formation in geophysical mass flows. J. Geophys. Res. 117, F01032. http://dx.doi.org/10.1029/2011JF002185.

Logan, M., Iverson, R.M., 2007, revised 2013. Video Documentation of Experiments at the USGS Debris-Flow Flume 1992–2006 (Amended to Include 2007–2013). v. 1.3. U.S. Geological Survey, Open-File Report, 2007-1315. http://pubs.usgs.gov/of/2007/1315/.

Major, J.J., 1997. Deposition al processes in large-scale debris-flow experiments. J. Geol. 105, 245–366.

Major, J.J., Iverson, R.M., 1999. Debris flow deposition: effects of pore-fluid pressure and frictions concentrated at flow margins. Geol. Soc. Am. Bull. 111, 1424–1434.

Pierson, T.C., Scott, K.M., 1985. Downstream dilution of a lahar: transition from debris flow to hyperconcentrated streamflow. Water Resour. Res. 21, 1511–1524.

Pierson, T.P., Janda, R.J., Thouret, J.C., Borerro, C.A., 1990. Perturbation and melting of snow and ice by the 13 November 1985 eruption of Nevado del Ruiz, Colombia, and consequent mobilization, flow and deposition of lahars. J. Volcanol. Geoth. Res. 41, 17–66.

Scott, K.M., 1988. Origins, Behavior, and Sedimentology of Lahars and Lahar-runout Flows in the Toutle-Cowlitz River System. U.S. Geological Survey, Professional Paper, 1447-A, 74 p.

Scott, K.M., Vallance, J.W., Kerle, N., Macías, J.L., Strauch, W., Devoli, G., 2005. Catastrophic precipitation-triggered lahar at Casita volcano, Nicaragua—occurrence, bulking, and transformation. Earth Surf. Proc. Land. 30, 59–79.

Vallance, J.W., Scott, K.M., 1997. The Osceola Mudflow from Mount Rainier: sedimentology and hazard implications of a huge clay-rich debris flow. Geol. Soc. Am. Bull. 109, 143–163.